# Constraining Dark Energy with X-ray Clusters, SNe Ia and the CMB

D. Rapetti
*Institute of Astronomy, Cambridge, CB3 OHA, UK*
*Departament d'Astronomia, Barcelona, 08028, Spain and*
*KIPAC, Stanford CA 94305-4060, USA*
S. W. Allen
*Institute of Astronomy, Cambridge, CB3 OHA, UK and*
*KIPAC, Stanford CA 94305-4060, USA*
J. Weller
*Institute of Astronomy, Cambridge, CB3 OHA, UK*
*FNAL, Batavia, IL 60510-0500, USA and*
*UCL, London WC1E 6BT, UK*

In [1] we present new constraints on the evolution of dark energy from an analysis of Cosmic Microwave Background, supernova and X-ray galaxy cluster data. From a combined analysis of all three data sets and assuming that the Universe is flat, we examine a series of dark energy models with up to three free parameters: the current dark energy equation of state $w_0$, the early time equation of state $w_{\rm et}$ and the scale factor at transition, $a_{\rm t}$. Allowing the transition scale factor to vary over the range $0.5 < a_{\rm t} < 0.95$ where the data sets have discriminating power, we measure $w_0 = -1.27^{+0.33}_{-0.39}$ and $w_{\rm et} = -0.66^{+0.44}_{-0.62}$. We find no significant evidence for evolution in the dark energy equation of state parameter with redshift. The complementary nature of the data sets leads to a tight constraint on the mean matter density, $\Omega_{\rm m}$, alleviates a number of other parameter degeneracies, including that between the scalar spectral index $n_{\rm s}$, the physical baryon density $\Omega_{\rm b}h^2$ and the optical depth $\tau$ and also allows us to examine models dropping the flatness prior. As required for the energy–momentum conservation our analysis includes spatial perturbations in the dark energy component. We show that not including them leads to spuriously tighter constraints on $w_0$ and especially on $w_{\rm et}$.

## 1. Introduction

The precise measurement of the Cosmic Microwave Background (CMB) made with the Wilkinson Microwave Anisotropy Probe (WMAP) [2–5] has improved our knowledge of a wide range of cosmological parameters. However, a number of degeneracies between parameters exist which cannot be broken with current CMB data alone and which require the introduction of other, complementary data sets. Some of the most important parameters and degeneracies concern dark energy and its equation of state. When describing the background evolution of the Universe with a such new component, it is sufficient to know its equation of state i.e. the ratio of pressure and energy density, $w = p_{\rm de}/\rho_{\rm de}$. Whilst a cosmological constant has $w = -1$ at all times, for most dark energy models the equation of state parameter is an evolving function of redshift, $w = w(z)$. In order to learn more about the origin of cosmic acceleration and dark energy, it is crucial to constrain the evolution of the dark energy equation of state.

The data for SNIa can be used to measure the luminosity distances to these sources independent of their redshifts. This constrains a combination of the dark matter and dark energy densities in a different way to observations of CMB anisotropies. The combination of the two data sets is therefore useful in breaking parameter degeneracies. However, in order to constrain the evolution of the equation of state with supernovae observations, it is necessary to use a tight prior on the mean matter density of the Universe, $\Omega_{\rm m}$. Recent measurements of the gas fraction in X-ray luminous, dynamically relaxed clusters made with the Chandra X-ray Observatory provide one of our best constraints on $\Omega_{\rm m}$ [7]. These data also provide a direct and independent method by which to measure the acceleration of the Universe, providing additional discriminating power for dark energy studies. The combination of CMB and X-ray cluster data plays also an important role in breaking other key parameter degeneracies. For these reasons, we have used a combination of X-ray gas fraction, CMB and SNIa data in this study.

In Section 2 we present our parameterization for the dark energy equation of state. In Section 3 we discuss the individual data sets and how they probe cosmology. Our results are presented in Section 4 and Section 5 summarizes our conclusions.

## 2. Dark Energy Model

We use an extension of the model discussed by [8] and [9]. The primary short-coming of this parameterization is that it uses a fixed redshift, $z = 1$, for the transition between the current value of the equation of state and the value at early times, $w_{\rm et} = w_0 + w_1$. Our model introduces one extra parameter: $z_{\rm t}$, the transition redshift between $w_{\rm et}$ and $w_0$, such that

$$w = \frac{w_{\rm et} z + w_0 z_{\rm t}}{z + z_{\rm t}} = \frac{w_{\rm et}(1-a)a_{\rm t} + w_0(1-a_{\rm t})a}{a(1-2a_{\rm t}) + a_{\rm t}} \ , \quad (1)$$

where $a_{\rm t}$ is the transition scale factor. Energy conservation of the dark energy fluid results in evolution of the energy density with the scale factor, such that

$$\rho_{\rm de}(a) = \rho_{\rm de,0} a^{-3} e^{-3\int_1^a \frac{w(a')}{a'} da'} , \quad (2)$$

where $\rho_{\rm de,0}$ is the energy density of the dark energy fluid today. Using the parameterization of equation (1) we obtain

$$\int_1^a \frac{w(a')}{a'} da' = w_{\rm et} \ln a + (w_{\rm et} - w_0) g(a; a_{\rm t}) \ , \quad (3)$$

with

$$g(a; a_{\rm t}) = \left(\frac{1-a_{\rm t}}{1-2a_{\rm t}}\right) \ln\left(\frac{a(1-a_{\rm t})}{a(1-2a_{\rm t}) + a_{\rm t}}\right) \ . \quad (4)$$

From the Friedmann equation, the evolution of the Hubble parameter $H(z) = H_0 E(z)$ is given by

$$E(z) = \sqrt{\Omega_{\rm m}(1+z)^3 + \Omega_{\rm de} f(z) + \Omega_{\rm k}(1+z)^2} \ , \quad (5)$$

with

$$f(z) = (1+z)^{3(1+w_{\rm et})} e^{-3(w_{\rm et} - w_0) g(z; z_{\rm t})}, \quad (6)$$

where $\Omega_{\rm m}$, $\Omega_{\rm de}$, $\Omega_{\rm k}$ are the matter, dark energy and curvature densities in units of the critical density.

## 3. Data Analysis

We have performed a likelihood analysis using three cosmological data sets: CMB, SNIa and the X-ray cluster gas fraction.

For the CMB analysis we have modified the CAMB[1] code [10] to include the relevant dark energy equation of state parameters. For the calculation of CMB spectra, we have included perturbations in the dark energy component [11]. We assume that the sound speed of the dark energy fluid, $c_{\rm s}^2 = 1$. We note the presence of an extra term in the perturbation equations due to the variation of the equation of state with time, which sources the density perturbation with the velocity perturbation. This effect will be discussed in a forthcoming publication [12]. We have included this extension of the CAMB code into the COSMOMC package, which provides an efficient sampling of the posterior likelihoods using a Markov Chain Monte Carlo (MCMC) algorithm [2] [13].

[1] http://camb.info
[2] http://cosmologist.info/cosmomc/

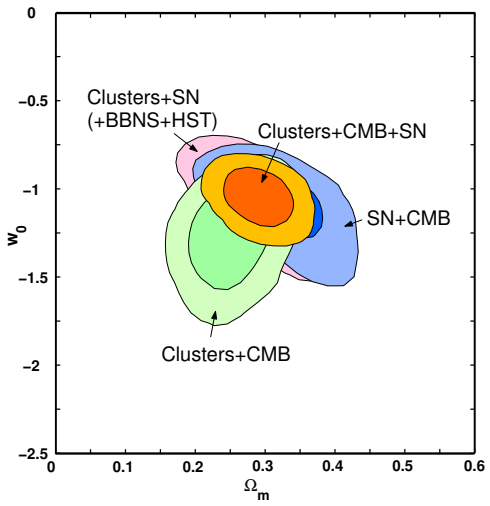


Figure 1: The 68.3 and 95.4 per cent confidence limits in the $(\Omega_{\rm m}, w_0)$ plane for the various pairs of data sets and for all three data sets combined. A constant dark energy equation of state parameter is assumed.

We use three CMB data sets: WMAP [2–4] (including the temperature-polarization cross-correlation data), the Cosmic Background Imager (CBI) [14] and the Arcminute Cosmology Bolometer Array Receiver (ACBAR) [15]. The latter data sets provide important information on smaller scales ($\ell > 800$).

For the SNIa analysis, we use the gold sample of [6], marginalizing analytically over the absolute magnitude $M$ as a "nuisance parameter". We fit the extinction-corrected distance moduli, $\mu_0 = m - M = 5\log d_L + 25$, where $m$ is the apparent magnitude and $d_L$ is the luminosity distance in units of Mpc defined as

$$d_L = \frac{c(1+z)}{H_0\sqrt{\Omega_k}} \sinh\left(\sqrt{\Omega_k}\int_0^z \frac{dz}{\sqrt{E(z)}}\right) \ , \quad (7)$$

where $\Omega_{\rm k} = 1 - \Omega_{\rm m} - \Omega_{\rm de}$.

For the X-ray gas mass fraction analysis, we use the data and method of [7], fitting the apparent redshift evolution of the cluster gas fraction with the model

$$f_{\rm gas}^{\rm SCDM}(z) = \frac{b\,\Omega_{\rm b}}{\left(1 + 0.19\sqrt{h}\right)\Omega_{\rm m}} \left[\frac{d_{\rm A}^{\rm SCDM}(z)}{d_{\rm A}^{\rm de}(z)}\right]^{1.5} \ , \quad (8)$$

where $d_{\rm A}^{\rm de}(z)$ and $d_{\rm A}^{\rm SCDM}(z)$ are the angular diameter distances ($d_A = d_L/(1+z)^2$) to the clusters for a given dark energy (de) model and the reference standard cold dark matter cosmology, respectively. $\Omega_{\rm b}$ is the mean baryonic matter density of the Universe in units of the critical density, $H_0 = 100\,h\,{\rm km\,sec^{-1}\,Mpc^{-1}}$ and $b$ is a bias factor that accounts for the (relatively small amount of) baryonic material expelled from galaxy clusters as they form. Following [7], we

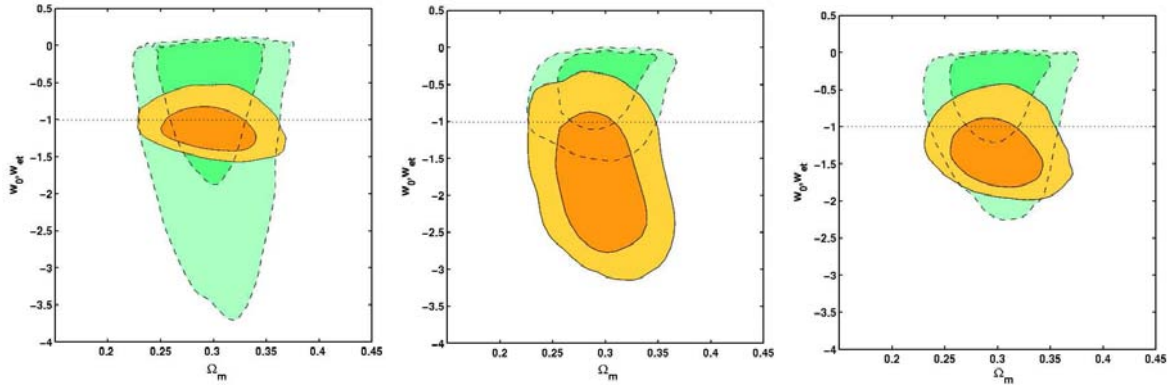


Figure 2: The 68.3 and 95.4 per cent confidence limits in the ($\Omega_{\rm m}$;$w_0$,$w_{\rm et}$) plane for all three data sets combined using various fixed values for the transition redshift. The solid lines show the results on ($\Omega_{\rm m}$,$w_0$). The dashed lines show the results on ($\Omega_{\rm m}$,$w_{\rm et}$). The left panel is for $z_{\rm t} = 1$ ($a_{\rm t} = 0.5$), the center panel $z_{\rm t} = 0.11$ ($a_{\rm t} = 0.9$) and the right panel $z_{\rm t} = 0.35$ ($a_{\rm t} = 0.74$). The uncertainty in $w_{\rm et}$ is much larger than for $w_0$ in the left panel, which reflects the paucity of data at high redshifts. The $z_{\rm t} = 0.35$ transition splits the cluster and SNIa data into similarly sized low and high redshift subsamples. The horizontal dotted line denotes the cosmological constant model ($w_0 = w_{\rm et} = -1$).

adopt a Gaussian prior on $b = 0.824 \pm 0.089$, which is appropriate for clusters of the masses studied here.

Except where stated otherwise, our analysis assumes that the Universe is flat ($\Omega_{\rm k} = 0$). For the analysis of the cluster data without the CMB data, we use Gaussian priors on $\Omega_{\rm b}h^2 = 0.0214 \pm 0.0020$ from Big Bang Nucleosynthesis (BBN) constraints [17] and $h = 0.72 \pm 0.08$ from observations made with the Hubble Space Telescope (HST) [18].

## 4. Dark Energy constraints

Figure 1 shows the constraints on $w_0$ and $\Omega_{\rm m}$ for constant dark energy equation of state. We see that the combination of the three data sets leads to tight constraints on $w_0$ and $\Omega_{\rm m}$, which are in good agreement with the cosmological constant scenario ($w_0 = -1$). This figure also demonstrates the complementary nature of the constraints provided by the various pairs of data sets, in particular SNIa+CMB and clusters+CMB.

We have also examined the constraints obtained using two free parameters for the dark energy equation of state, $w_0$ and $w_{\rm et}$, and different fixed values of $z_{\rm t}$ ($a_{\rm t}$). The left panel of Figure 2 shows the results using a parameterization with a redshift transition $z_{\rm t} = 1$, which coincides with the parameterization proposed by [8] and [9]. The center panel shows the constraints using a late transition model with $z_{\rm t} = 0.11$ ($a_{\rm t} = 0.9$). We see that the cosmological constant ($w_0 = w_{\rm et} = -1$) again lies within the allowed 68.3 per cent confidence ($1\sigma$) regions. Unsurprisingly, the constraints on $w_{\rm et}$ in the late transition case are better than for the $z_{\rm t} = 1$ model, reflecting the presence of more cluster and SNIa data beyond the transition redshift. Naturally, this at the expense of a weaker constraint on $w_0$.

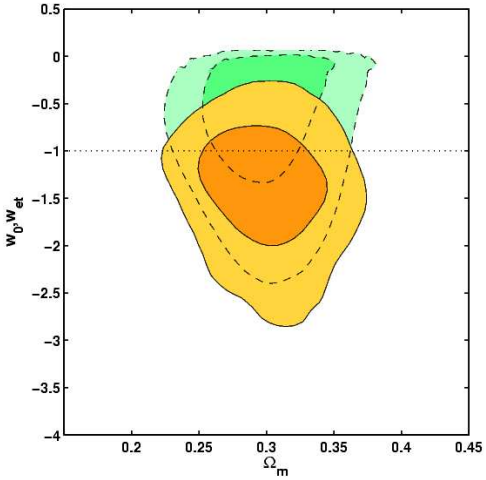


Figure 3: The 68.3 and 95.4 per cent confidence limits in the ($\Omega_{\rm m}$;$w_0$,$w_{\rm et}$) plane for a dark energy model with three free parameters. The solid lines show the results on ($\Omega_{\rm m}$,$w_0$). The dashed lines show the results on ($\Omega_{\rm m}$,$w_{\rm et}$). The horizontal dotted line denotes the cosmological constant model ($w_0 = w_{\rm et} = -1$).

If we select a transition redshift close to the median redshift for the SNIa and cluster data sets, one might expect to obtain comparable constraints on $w_0$ and $w_{\rm et}$. In principle, this approach could provide improved sensitivity when searching for evolution in the equation of state parameter. (In detail, we expect the constraints on $w_0$ to be slightly better than those for $w_{\rm et}$ using the median redshift model, since the precision of the individual cluster and supernova measurements are lower at high redshifts.) The right panel of Figure 2 shows the results obtained fixing

Table I The median parameter values of the marginalized probability distributions (and 68.3 per cent confidence intervals) for various dark energy parameterizations, using all three data sets combined. Results are listed for both flat and non-flat priors. The last column states the $\chi^2$ per degree of freedom for each parameterization.

| **equation of state** | $w_0$ | $w_{\rm et}$ | $\Omega_{\rm m}$ | $\chi^2$/dof |
|---|---|---|---|---|
| constant (flat) | $-1.051^{+0.098}_{-0.119}$ | - | $0.295^{+0.031}_{-0.027}$ | 1652.5/1534 |
| constant (non flat) | $-1.092^{+0.121}_{-0.147}$ | - | $0.314^{+0.040}_{-0.036}$ | 1651.3/1533 |
| $z_{\rm t} = 1$ (flat) | $-1.097^{+0.229}_{-0.189}$ | $-0.866^{+0.613}_{-1.098}$ | $0.300^{+0.029}_{-0.028}$ | 1650.6/1533 |
| $z_{\rm t} = 1$ (non flat) | $-1.078^{+0.305}_{-0.227}$ | $-1.229^{+0.863}_{-2.058}$ | $0.328^{+0.046}_{-0.040}$ | 1648.1/1532 |
| split, $z_{\rm t} = 0.35$ (flat) | $-1.298^{+0.343}_{-0.281}$ | $-0.605^{+0.403}_{-0.620}$ | $0.300^{+0.028}_{-0.027}$ | 1649.0/1533 |
| arbitrary $z_{\rm t}$ (flat) | $-1.269^{+0.332}_{-0.394}$ | $-0.664^{+0.435}_{-0.616}$ | $0.299^{+0.029}_{-0.027}$ | 1648.9/1532 |

$z_{\rm t} = 0.35$ ($a_{\rm t} = 0.74$), a redshift close to the median redshift for both the cluster and SNIa data sets. In this case the uncertainties on $w_0$ and $w_{\rm et}$ are indeed similar and the combined size of the confidence regions is reduced. However, the cosmological constant remains an acceptable description of the data. The marginalized results on $w_0$, $w_{\rm et}$ and $\Omega_{\rm m}$ are summarized in Table I.

The most general dark energy model we have examined includes $w_0$, $w_{\rm et}$ and the transition scale factor, $a_{\rm t}$, as free parameters. Figure 3 shows the confidence contours in the ($\Omega_{\rm m}$;$w_0$,$w_{\rm et}$) plane. The marginalized results on $w_0$, $w_{\rm et}$ and $\Omega_{\rm m}$ are summarized in Table I. Again, the results obtained with our most general dark energy model are consistent with a cosmological constant. Note that the CMB data provide an upper limit of $w_{\rm et} \lesssim 0$ at high redshifts; for $w_{\rm et} > 0$, the dark energy component would become significant at early times, causing modifications to the predicted CMB anisotropy spectrum.

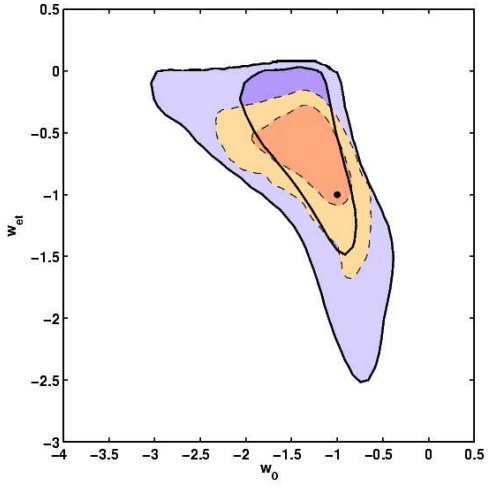


Figure 4: The 68.3 and 95.4 per cent confidence limits in the ($w_0$,$w_{\rm et}$) plane obtained from analyses which account for (blue, solid contours; as in Fig 3) or incorrectly neglect (red, dashed contours) the effects of dark energy perturbations. The model used incorporates a free transition redshift for the dark energy equation of state and is fitted to all three data sets: clusters+SNIa+CMB.

## 4.1. The relevance of including dark energy perturbations

As mentioned above, our analysis accounts for the effects of spatial fluctuations in the dark energy component. Most previous studies have not accounted for these perturbations, despite the fact that this leads to violation of energy–momentum conservation whenever dark energy is not a cosmological constant [19, 20]. It is important to ask whether the inclusion of these perturbations has a significant effect on the results; it has been argued by some authors that dark energy perturbations can be neglected if the equation of state remains around the cosmological constant value. However, we find that for an evolving equation of state, neglecting the effects of such perturbations can lead to spuriously tight constraints on the dark energy parameters.

For a constant equation of state, [11] showed that the inclusion of dark energy perturbations leads to an opening up of the ($\Omega_{\rm m}$,$w_0$) contours, allowing more negative values of $w_0$. Repeating their analysis using our three data sets (clusters+SNIa+CMB) we measure a reduced effect, due to the complementary nature of our data sets. Neglecting the effects of dark energy perturbations leads to only a small shift in the marginalized probability distribution for $w_0$ and slightly tighter constraints ($w_0 = -0.988^{+0.095}_{-0.106}$; see Table I for the results obtained including perturbations).

For our most general, evolving dark energy model, however, the effects of perturbations in the dark energy component are more important and neglecting them can lead to spuriously tight constraints. Figure 4 compares the results in the ($w_0$,$w_{\rm et}$) plane obtained when including dark energy perturbations (solid contours) or neglecting them (dashed contours). When the effects of dark energy perturbations are wrongly ignored, we obtain spuriously tight constraints on $w_0 = -1.250^{+0.250}_{-0.335}$ and especially $w_{\rm et} = -0.671^{+0.213}_{-0.298}$;

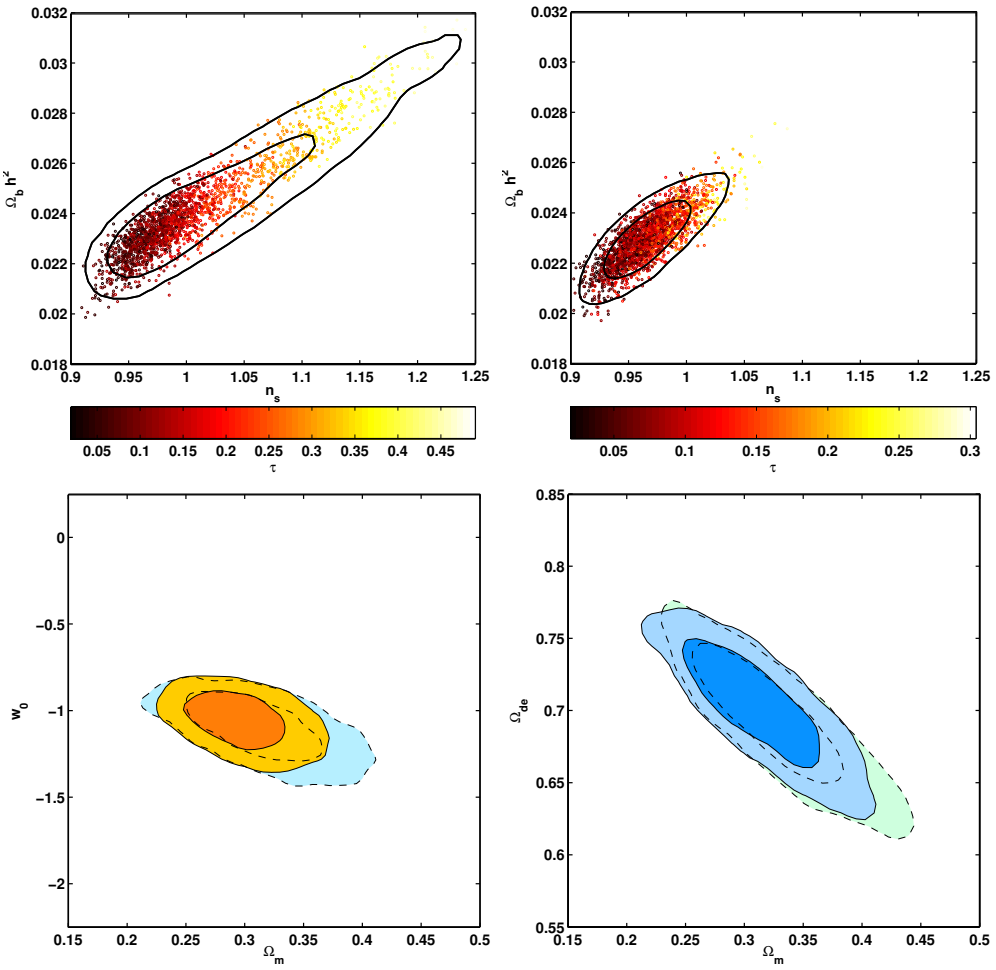


Figure 5: (Top panels) The 68.3 and 95.4 % confidence limits in the $(n_s, \Omega_{\rm b}h^2)$ plane either using SNIa+CMB data (left panel) or clusters+CMB data (right panel). The combination of clusters+CMB data alleviates the degeneracies between these parameters. (Bottom panels) The $(\Omega_{\rm m}, w_0)$ plane using all three data sets, assuming either a flat prior (solid contours) or not (dashed contours). The left panel shows the $(\Omega_{\rm m}$,$\Omega_{\rm de})$ plane from the analysis of the combined cluster+SNIa+CMB data set, with $\Omega_k$ included as a free parameter. The solid contours show the constraints for constant $w$. The dashed contours show the results for the $z_{\rm t} = 1$ dark energy model.

the apparent uncertainties in the latter are reduced by a factor of $\sim 2$ from the values in Table I. Figure 4 also shows that when we incorrectly neglect the effects of dark energy perturbations, the sharp boundary provided by the CMB data set around $w_{\rm et} \sim 0$ is not reached.

## 4.2. Breaking degeneracies with data instead of priors

One of the main parameter degeneracies highlighted in previous studies [21] is between the scalar spectral index $n_s$, the physical baryon density $\Omega_{\rm b}h^2$ and the optical depth to reionization, $\tau$; this degeneracy impinges on the measured dark energy parameters. As noted by [21], the integrated Sachs-Wolfe effect in the case of an evolving dark energy equation of state increases the importance of this degeneracy with respect to constant $w$ models. The top left panel of Fig 5 shows this degeneracy for the case of the SNIa+CMB data, using the $z_{\rm t} = 0.35$ dark energy model. The top right panel shows how the degeneracy is lessened when the clusters+CMB data are used.

The combination of clusters+CMB data even allows us to relax the assumption that the Universe is flat, although we note that the computation of MCMC chains in the non-flat case is time consuming when one wishes to ensure convergence. (For this reason, we have only carried out a limited exploration of non-flat models here.) In order to avoid unphysical regions of the parameter space when using non-flat models, we have also included a prior on the optical depth to reionization, $\tau < 0.3$, in a similar manner to WMAP

team [5] and [21]. The bottom left panel of Figure 5 shows the 68.3 and 95.4 per cent confidence limits in the ($\Omega_{\rm m}$,$w_0$) plane obtained assuming a constant dark energy equation of state, with the curvature included as a free parameter. Comparison with Figure 1 shows that the uncertainties in the parameters are increased when the assumption of flatness is dropped. However, we still have clear evidence that $w_0 < -1/3$ and therefore that the Universe is accelerating at late times. We obtain tight constraints on $\Omega_{\rm k} = -0.017^{+0.020}_{-0.021}$, $\Omega_{\rm m} = 0.314^{+0.040}_{-0.036}$ and $\Omega_{\rm de} = 0.703^{+0.026}_{-0.030}$. The bottom right panel of Figure 5 shows the results in the ($\Omega_{\rm m}$,$\Omega_{\rm de}$) plane for constant $w$ (solid contours) and for the $z_{\rm t} = 1$ dark energy model (dashed contours).

## 5. Conclusions

The combined analysis of X–ray cluster, SNIa and CMB data is a powerful tool to constrain dark energy (see Table I). Employing a series of dark energy models with up to three free parameters ($w_0$, $w_{\rm et}$ and $z_{\rm t}$) we find no significant evidence for evolution in the equation of state. A cosmological constant is a good description of the current data.

Rather than using strong priors, our approach has been to use a combination of data sets that are complementary in nature and which allow certain key parameter degeneracies to be alleviated (see Figure 5).

For models other than a cosmological constant, we have included the effects of perturbations in the dark energy component to avoid violating energy–momentum conservation. We have shown that neglecting perturbations can lead to spuriously tight constraints on dark energy models, especially for the $w_{\rm et}$ parameter (by up to a factor two for our most general model).

Further Chandra observations of X-ray luminous, high-redshift, dynamically relaxed clusters should lead to rapid improvements in the constraints from the X-ray method. Continual progress in SNIa studies is expected over the next few years and the forthcoming, second release of WMAP data should, at the very least, provide an important, overall tightening of the constraints.

In the long term, the combination of complementary constraints from missions such as Constellation-X, SNAP and Planck, combining high precision with a tight control of systematic uncertainties, offers our best prospect for understanding the nature of dark energy.

## Acknowledgments

The authors wish to thank A. Lewis, S. Bridle and P. S. Corasaniti for helpful discussions and R. M. Johnstone and S. Rankin for technical support. The computational analysis was carried out using the Cambridge X-ray group Linux cluster and the UK National Cosmology Supercomputer Center funded by SGI, Intel, HEFCE and PPARC. DR is funded by an EARA Marie Curie Training Site Fellowship under the contract HPMT-CT-2000-00132. DR wishes to thank KIPAC, SLAC and Stanford University for hospitality during his visit there. SWA thanks the Royal Society for support at Cambridge. JW is supported by the DOE and the NASA grant NAG 5-10842 at Fermilab.

## References

[1] Rapetti D., Allen S. W., Weller J., 2004, preprint (astro-ph/0409574)
[2] Hinshaw G., et al., 2003, ApJ S., 148, 135
[3] Kogut A., et al., 2003, ApJ S., 148, 161
[4] Verde L., et al., 2003, ApJ S., 148, 195
[5] Spergel D. N., et al., 2003, ApJ S., 148, 175
[6] Riess A. G., et al., 2004, ApJ, 607, 665
[7] Allen S. W., Schmidt R. W., Ebeling H., Fabian A. C., van Speybroeck L., 2004, MNRAS, 353, 457
[8] Chevallier M., Polarski D., 2001, Int. J. Mod. Phys., D10, 213
[9] Linder E. V., 2003, Phys. Rev. Lett., 90, 091301
[10] Lewis A., Challinor A., Lasenby A., 2000, Astrophys. J., 538, 473
[11] Weller J., Lewis A. M., 2003, MNRAS, 346, 987
[12] Rapetti D., Weller J., 2005, to be published
[13] Lewis A., Bridle S., 2002, Phys. Rev.D, 66, 103511
[14] Pearson T. J., et al., 2003, Astrophys. J., 591, 556
[15] Kuo C. L., et al., 2004, Astrophys. J., 600, 32
[16] Riess A., et al., 1998, Astron. J, 116, 1009
[17] Kirkman D., Tytler D., Suzuki N., O'Meara J. M., Lubin D., 2003, ApJ S., 149, 1
[18] Freedman W., et al., 2001, ApJ, 553, 47
[19] Hu W., 2004, preprint (astro-ph/0410680)
[20] Caldwell R. R., Doran M., 2005, preprint (astro-ph/0501104)
[21] Corasaniti P. S., Kunz M., Parkinson D., Copeland E. J., Bassett B. A., 2004, Phys. Rev.D, in press (astro-ph/0406608)